Polymer 49 (2008) 3770–3779

Contents lists available at ScienceDirect

Polymer

journal homepage: www.elsevier.com/locate/polymer

Reactive patterning via post-functionalization of polymer brushes utilizing disuccinimidyl carbonate activation to couple primary amines

Steve Diamanti [a], Shafi Arifuzzaman [b], Andrea Elsen [a], Jan Genzer [b], Richard A. Vaia [a,*]

[a] Air Force Research Laboratory, Materials and Manufacturing Directorate, 2941 Hobson Way, Wright–Patterson Air Force Base, OH 45433-7750, United States
[b] North Carolina State University, Department of Chemical and Biomolecular Engineering, 911 Partners Way, Raleigh, NC 27695-7905, United States

ARTICLE INFO

Article history:
Received 3 June 2008
Accepted 9 June 2008
Available online 18 June 2008

Keywords:
Post-functionalization
Polymer brush
Patterning

ABSTRACT

Polymer brushes provide an exceptional route to surface functionalization due to their chemical and mechanical robustness, lack of large-area defects, and high density of functional groups. In spite of these benefits, the synthetic difficulty and complex surface structure associated with polymer brushes have hindered their utilization for constructing multifunctional, patterned surfaces. In this contribution we describe the use of a rapid and highly efficient polymer brush post-functionalization technique as a facile method for controlling surface functionality of polymer brushes. Poly(2-hydroxyethyl methacrylate) (PHEMA) brushes are post-functionalized via activation with *N*,*N*′-disuccinimidyl carbonate (DSC) and subsequent coupling to molecules containing α-amine moieties. This post-functionalization effectively tailors surface energy resulting in water contact angles ranging from 40° to 100° using different conjugate molecules. Furthermore, the solvent tolerance, insensitivity to reactant concentration, and rapid reaction time of the aminolysis reaction enable surface energy patterning of the polymer brushes through the use of "reactive" soft lithography. Finally, these surface energy patterns could be "developed" by exposure to gold nanoparticle solutions to yield surfaces with patterned nanoparticle density.

Published by Elsevier Ltd.

1. Introduction

Tailoring the surface chemistry of solid substrates by synthetic tools is of fundamental importance in materials science, for example in the creation of biologically relevant interfaces for sensing and separation applications [1]. Popular methods of tuning surface functionality are based on decorating surfaces with self-assembled monolayers (SAMs), polymer thin films, and polymer brushes [2]. SAMs have been extensively studied due to their molecular order and synthetic simplicity [3]. Polymer brushes share many of the same characteristics as SAMs but offer distinct advantages including the ability to tailor surface coverage, thickness, and composition, and increased functional group density and robustness [4]. The main drawback of polymer brushes has been the technical difficulty associated with their synthesis. In particular, tuning the surface functionality of polymer brushes requires the use of different monomers, which necessitates tailoring of the polymerization methodology for each monomer choice in order to achieve the desired grafting density and chain length. The structural complexity of polymer brushes and the complexity associated with tailoring their surface properties have led to the preferential use of SAMs for patterning applications.

An alternate method of tuning polymer brush surface properties is through post-functionalization from a common polymer brush platform. This route for the generation of functional brushes allows the fabrication of a wide variety of surface functionalities without changing polymerization kinetics and enables incorporation of chemical moieties or creation of polymer architectures that are not tolerated by the polymerization process [5]. Although there have been extensive reports of derivatization of free polymer chains, there have been only a handful of reports on the side chain and chain end functionalization of tethered polymer brushes [6]. Although end-group functionalization may be preferable in cases where 1:1 ligand/receptor stoichiometry is required, the higher density of side chains provides a greater ability to impact surface properties, enable multidentate interactions, and achieve full surface passivation. The majority of previous attempts at polymer brush post-functionalization have focused on the coupling of specific molecules, rather than broad-range reactivity. A notable exception is the recent work by Murata et al., which involved the synthesis of polymers with succinimide side chains and subsequent coupling of a broad range of functional amines [7]. Unfortunately, this approach relies on a succinimide substituted-monomer, which had to be specially synthesized. The authors did not attempt to use this post-functionalization approach for surface patterning; however, the

* Corresponding author. Tel.: +1 937 255 9209; fax: +1 937 255 9157.
E-mail address: richard.vaia@wpafb.af.mil (R.A. Vaia).

0032-3861/$ – see front matter Published by Elsevier Ltd.
doi:10.1016/j.polymer.2008.06.020

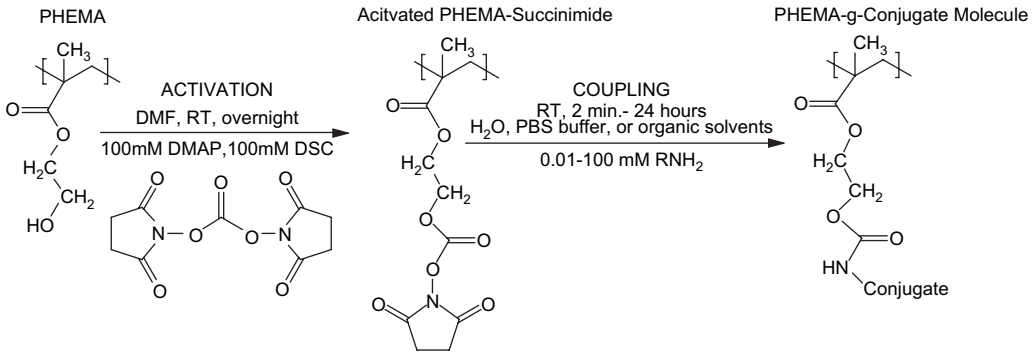

Fig. 1. Functionalization of PHEMA side chain using DSC activation and subsequent amination.

timescale of the aminolysis reaction (≈16 h) is not amenable to patterning where it is essential to have a relatively rapid, technically simple, and highly efficient coupling chemistry.

Another approach to post-polymerization functionalization is to utilize a two-step process, in which an existing moiety on the polymer side chain is selectively "activated" then subsequently coupled to by a rapid, orthogonal reaction. The activation-coupling approach is conceptually amenable to the creation of complex brush architectures and surface patterns. For example, after spatially uniform activation, the subsequent coupling reaction could be spatially confined. Steric bulk and diffusivity could potentially be harnessed to enable control of coupling efficiency and the tailored distribution of large and small molecules perpendicular to the brush axis. Herein, we developed the activation-coupling approach based on the activation of the hydroxyl group of poly(2-hydroxyethyl methacrylate) (PHEMA) side chains with *N,N′*-disuccinimidyl carbonate (DSC) followed by subsequent coupling to a primary amine (Fig. 1). This coupling chemistry has been used extensively in the PEGylation of proteins and drugs, affinity column preparation, and solid-phase synthesis of peptide carbamates; it has thereby been demonstrated to be highly specific in its reactivity to α-amino groups, as well as its tolerance to a wide variety of solvents and biological buffers [8,9]. Furthermore, this DSC-mediated amination technique has been shown by several studies to give higher coupling yields with less side reactions than the *p*-nitrophenyl chloroformate (NPC) and 1,1′-carbonyldiimidazole (CDI) mediated coupling reactions used by previous polymer brush post-functionalization approaches [9]. The carbamate linkage yielded by the two-step activation-coupling approach is known to have higher stability toward hydrolysis and proteolysis than moieties commonly obtained by one-step processes, such as, amide or ester linkages [10]. This highly versatile methodology has allowed us to study the effect of post-functionalization of a variety of conjugate molecules on the surface properties of PHEMA brushes and to pattern the surface energy of a polymer brush substrate via post-functionalization.

1.1. Post-functionalization

PHEMA brushes were synthesized on silicon wafers via the grafting from method utilizing atom transfer radical polymerization (ATRP) [11]. This synthesis of PHEMA followed the route suggested by Robinson and coworkers [12]. Details of the synthesis and associated characterization are provided in Section 3, [11,21,22]. Specifically the post-functionalization discussed herein was performed on PHEMA chains (MW ≈ 12–15 kDa) end-tethered at ≈0.4–0.5 chains/nm^2. These characteristics result in a dry brush within the semidilute region, that is one that is swellable by a low molecular weight medium [13]. As shown previously, this synthetic scheme enabled the generation of linear (uncross-linked) PHEMA chains [11]. This is important as the hydroxyl terminus in the pendant group of each monomer is available for subsequent chemical functionalization, described in detail below.

To activate the brush, the substrate is immersed in a 100 mM solution of *N,N′*-disuccinimidyl carbonate (DSC) and 4-(dimethylamino)pyridine (DMAP) in anhydrous dimethylformamide (DMF) for up to 24 h. DMAP acts as a catalytic base, deprotonating the hydroxyl group, and thus making it more reactive towards DSC. The activated hydroxyl group then acts as a nucleophile and attacks the electrophilic carbonyl of DSC causing the formation of the activated succinimidyl group (Fig. 1). The brush is then taken out of solution and rinsed thoroughly with anhydrous DMF and methylene chloride in order to remove unreacted DSC/DMAP. Due to the small size of the succinimidyl carbonate group, only a modest increase in brush thickness is seen upon brush activation (Table 1, Entry 2).

Table 1
Post-functionalization of brushes with various functional groups

	Thickness[a] (nm)	Contact angle[b]	Composition[c]	100% coupling composition[d]	Coupling efficiency (%)[e]
PHEMA	14.8 ± 0.1	58 ± 2°	68% C, 32% O	67% C, 33% O	N/A
DSC–PHEMA	17.2 ± 0.2	65 ± 2°	62% C, 35% O, 3% N	58% C, 37% O, 5% N	~90[f]
PHEMA-*g*-C_{16}	22.4 ± 0.2	99 ± 1°	81% C, 16% O, 3% N	82% C, 14% O, 4% N	87 ± 11
PHEMA-*g*-PEG_{20}	23.8 ± 0.3	43 ± 1°	67% C, 31% O, 2% N	66% C, 32% O, 2% N	79 ± 5
PHEMA-*g*-PEG_{50}	20.8 ± 0.3	38 ± 1°	65% C, 34% O, 1% N	66% C, 33% O, 1% N	43 ± 6
PHEMA-*g*-C_8F_{15}	20.7 ± 0.2	110 ± 1°	47% C, 18% O, 3% N, 32% F	43% C, 11% O, 3% N, 43% F	59 ± 6
C16 control[g] no activation	14.6 ± 0.3	60 ± 1°	66% C, 34% O	67% C, 33% O	–

All reactions in table performed on the same PHEMA brush substrate.
[a] Thickness measured by ellipsometry.
[b] Water contact angle.
[c] Elemental composition measured by XPS.
[d] Expected elemental composition at 100% coupling efficiency.
[e] As estimated from XPS data by comparing experimentally measured elemental composition and composition at 100% coupling or by carbon deconvolution for PEG coupled materials see Section 3 for full details.
[f] Estimated maximum activation efficiency based on coupling data.
[g] Unactivated brush was exposed to hexadecylamine solution for 24 h.

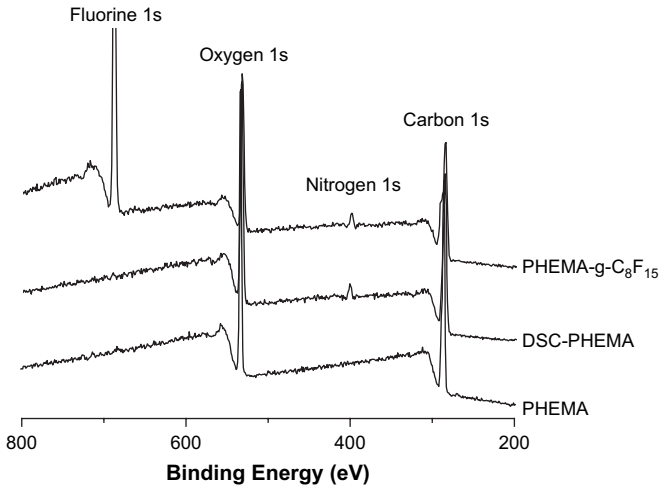

Fig. 2. XPS survey scans of pristine PHEMA brush, activated brush, and fluorinated conjugate.

This thickness increase is due to the increased steric constraints caused by the increased volume of side chain functional groups which cause an upward expansion of the individual chains to minimize steric repulsion [1,6i]. The activation step was found to be relatively slow, requiring at least 7 h for completion (Supplementary data). X-ray photoelectron spectroscopy (XPS) of the activated brush exhibits a nitrogen peak in the survey scan, providing qualitative confirmation of the conversion of a portion of the PHEMA hydroxyl side chain to the succinimidyl carbonyl activated side chain (Fig. 2). Unfortunately, direct quantification of activation efficiency is difficult due to the inherent inaccuracy of integrating the relatively small nitrogen peak or deconvoluting the contribution of the carbonyl peak to the carbon 1s peak. Subsequent coupling of α-amino molecules (Table 1) implies that the maximum activation efficiency in the near surface region of the brush must be ≥90%.

Coupling of α-amino molecules was achieved by immediately immersing the activated brush in a 0.010–100 mM solution of the reactant of choice for up to 24 h. After sonication and washing to desorb non-specifically bound reactants, the coupling of conjugate molecules resulted in an increase in brush thickness as measured by ellipsometry (Table 1, Entries 3–6). Furthermore, successful coupling was also demonstrated by a change in static water contact angle for conjugate molecules that were either more hydrophilic or hydrophobic than PHEMA (Table 1). In particular, the coupling of hydrophilic conjugates, such as PEG_{50} caused a substantial decrease in water contact angle (Table 1, Entry 4), while the coupling of a hydrophobic conjugate, such as hexadecylamine, caused a substantial increase in water contact angle (Table 1, Entry 3). In concert, the affinity of the surface to nanoparticle adsorption can be tuned. Fig. 3 shows the change in surface coverage of 30 nm citrate coated Au NPs on surfaces comprised of various α-amino molecules coupled to PHEMA brushes. Perflouro-functionalization created a surface that was completely repulsive to Au NP absorption. PEG functionalized surfaces demonstrated a marked increase in Au NP absorption relative to unfunctionalized PHEMA or alkane functionalized PHEMA. Higher molecular weight PEG showed greater affinity than lower molecular weight PEG. For PEG_{50}, reversible colorimetric detection of solvent vapor that swells the brush was observed due to the increase (decrease) in the mean Au NP spacing upon absorption (desorption) of the solvent, and associated hypsochromic (bathochromic) shifting of the collective plasmon resonance.

The extent of post-functionalization in approximately the upper third of the brush (Table 1) can be estimated using XPS either from the elemental composition, or in cases where elemental composition of the conjugate and PHEMA are very similar (as in PHEMA-*g*-PEG), by deconvolution of the carbon 1s peak which reveals the relative amounts of C–C, C–O, and C═O bonds (Fig. 4). For example, a fluorinated conjugate shows distinct nitrogen and fluorine peaks in the XPS survey scan (Fig. 2), reflecting the covalent attachment of this molecule to the brush. Furthermore, Fig. 4 compares the C1s peak for the pristine PHEMA brush with the PHEMA grafted hexadecylamine (PHEMA-*g*-C_{16}) and PHEMA grafted PEG_{50} (PHEMA-*g*-PEG_{50}). The expected proportions of C–C, C–O, and C═O (3:2:1) bonds are observed for PHEMA (Fig. 4A). When a primary alkane molecule (hexadecylamine) is coupled, a large increase in the relative amount of the low binding energy peak (C–C) is seen (Fig. 4B). In contrast, when PEG_{50}, containing a high density of ether linkages is coupled, a substantial increase in the proportion of peaks stemming from C–O bonds is noted (Fig. 4C). Note that a control experiment, in which pristine PHEMA brush is reacted directly with hexadecylamine without DSC activation, does not reveal substantial changes in thickness, contact angle, or elemental composition (Table 1, Entry 7). Similar results were seen in control experiments using the other reactants. Overall, these results demonstrate that DSC activation causes a specific reaction with primary amines and that the physical and elemental changes noted are not simply due to non-specific adsorption of reactant molecules. Finally, a variety of small peptides and other synthetic molecules have been coupled using the aforementioned procedure (Supplementary data).

Ellipsometry, XPS and changes in physical properties, including water contact angle, confirm the applicability of DSC activation for coupling α-amino molecules to PHEMA. Unfortunately, only limited understanding with regard to the final distribution of pendants along the chain axis is currently available. Attenuated Total Reflectance-IR confirmed the formation of succinimide and amide groups during the post-functionalization. However, due to the thin brush (<20 nm) and resultant poor signal-to-noise, the compositional analysis of the brush was less reliable than the analysis obtained by XPS. Attempts at depth profiling with XPS were inconclusive, attributed to the different etched rates of the elements artificially enriching compositions of the slower etching species. Variable take-off angle XPS was also found challenging due to the different mean-free path lengths of the 1s electrons. Previous studies have also cautioned independent use of these approaches, especially since conformation of brushes in dry state (ala vacuum) differs from that in solution (reaction) [14]. Future studies using X-ray and neutron reflectometry, as well as near edge X-ray absorption fine structure (NEXAFS) are necessary to elucidate the compositional variation along the brush axis.

Minimizing reactant concentration and reaction time, as well as, expanding potential reaction media are critical to optimizing the amination reaction for patterning applications. A substantial advantage of the DSC activation reaction is the purported stability of the activated group to water, making it amenable to coupling α-amines in water, thus enabling conjugation of biological molecules [9]. Nevertheless, many potential reactants have greater solubility in other media. In order to ascertain the effect of solvent on coupling efficiency, MeO–PEG_{20}–NH_2 was reacted with an activated brush in three different solvents (chloroform, acetone, and 50 mM phosphate buffered saline (PBS)). Coupling in acetone yields the largest increase in brush thickness, while chloroform and PBS buffer show similar brush thicknesses by ellipsometry (Table 2). The greater coupling efficiency measured by XPS (Table 2) from coupling in acetone (≈89%) versus chloroform and PBS (≈80%) could be due to the greater solubility of PEG in acetone, which yields a looser polymer coil with greater accessibility of the amine terminus for the coupling reaction. However, we do not find deleterious effects on the reaction from using any particular solvent, rather finding the optimal solvent for each set of reactions entails optimizing the solubility of the reactant.

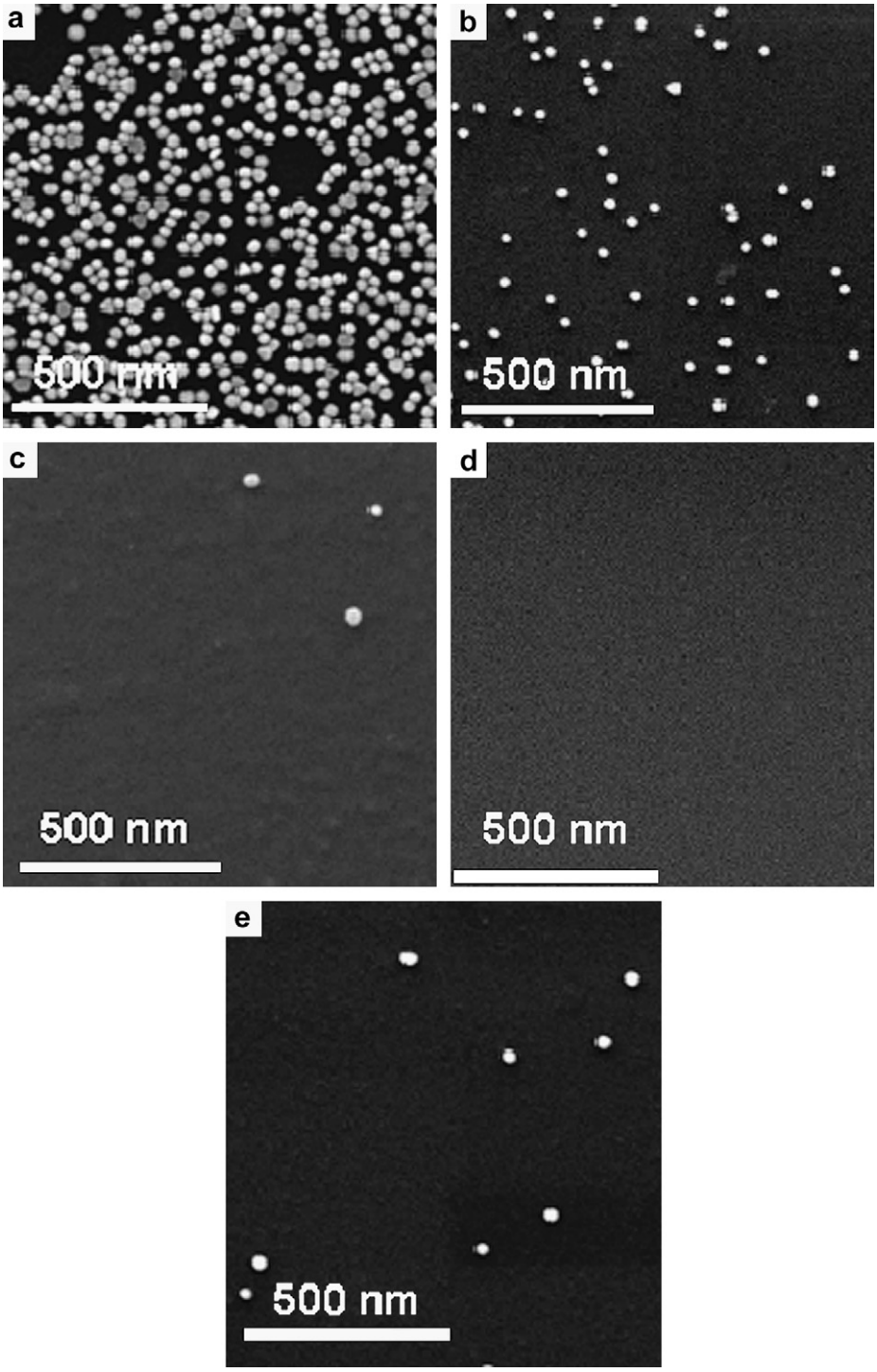

Fig. 3. Relative affinity of post-functionalized PHEMA brushes to adsorption of 30 nm citrate-capped Au nanoparticles. (a) PHEMA-*g*-PEG_{50} (130 ± 15 NP/μm^2); (b) PHEMA-*g*-PEG_{20} (41 ± 6.8 NP/μm^2); (c) PHEMA-*g*-C_{16} (0.8 ± 0.2 NP/μm^2); (d) PHEMA-*g*-C_8F_{15} (0 NP/μm^2); (e) pristine PHEMA (3.2 ± 1.8 NP/μm^2).

Paralleling the toleration of a range of reaction media, the surface amination reaction is also seen to be insensitive to reactant concentration and time (Supplementary data). For example, coupling of hexadecylamine in acetone for 24 h was effectively invariant in the concentration range of 10–50 mM, potentially decreasing slightly for low μM concentrations, as revealed by a minute decrease in brush thickness (ellipsometry). For 25 mM solutions of hexadecylamine in acetone, increase in brush thickness demonstrated substantial reaction progress in only 2 min with a plateau reached at 15 min. The water contact angle indicated a complete change to the equilibrium value in 2 min. This rapid change of surface properties suggests a reaction mechanism, by which surface groups react quickly and internal brush functionalities react more slowly due to the need for reactants to diffuse into the dense brush layer. Such diffusional limitation of polymer brush side-chain reactivity has been noted in other studies [7]. Multivariable optimization of concentration and contact time provides a wide range of processing conditions amenable for reactive contact printing (locally high reactive ink concentration and short contact time).

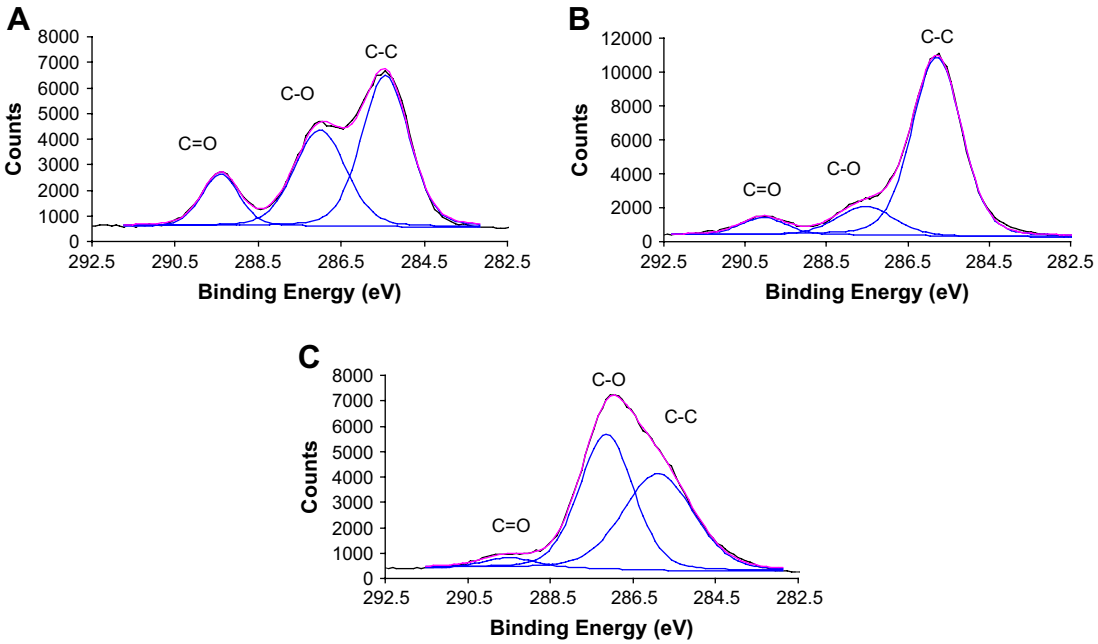

Fig. 4. Deconvoluted carbon 1s peak of pristine PHEMA brush (A), hexadecane conjugate (B) and PEG_{50} conjugate (C).

Table 2
Effect of solvent on extent of amination reaction

	Reaction solvent	Thickness[a] (nm)	Coupling efficiency[b]
PHEMA	–	15.0 ± 0.2	–
PHEMA-g-PEG_{20}	Acetone	26.2 ± 0.3	89 ± 6
PHEMA-g-PEG_{20}	Chloroform	24.0 ± 0.2	80 ± 5
PHEMA-g-PEG_{20}	PBS buffer	22.9 ± 0.2	79 ± 8

[a] Thickness measured by ellipsometry.
[b] As estimated from XPS data by carbon 1s peak deconvolution, see Section 3 for full details.

1.2. Reactive microcontact printing

The rapid reaction of the activated PHEMA brushes and insensitivity to reactant concentration imply that this process is amenable to "reactive" microcontact printing (R-μCP). Typically, μCP is performed on bare, inorganic surfaces for the formation of patterned SAMs. Patterns on a surface are formed via the deposition of material from an inked stamp, followed by the formation of covalent linkages with the surface via extremely efficient reactions, such as, gold–thiol or siloxane bond formation [15]. There have been far fewer examples of R-μCP on organically-derivatized SAMs in the literature, compared to conventional μCP [16,17]. An early example by Whitesides involved the printing of polymer chains onto a carboxylic anhydride activated substrate [15]. Recently, Huck et al. reported catalyst-free R-μCP of *N*-protected amino acids onto amino-functionalized SAMs and Reinhoudt et al. reported catalyst-free click reactions via R-μCP [16b,c]. Very recently there has been interest in the extension of R-μCP from SAMs to polymer thin films [18]. In general, these approaches have focused on cell-growth applications.

The aforementioned "activate and couple" process was utilized to enable R-μCP of organic molecules onto activated polymer brushes as detailed below and described schematically in Fig. 5. As a specific example, the PHEMA brush was activated as described above (Fig. 5, step 1). A PDMS stamp pattern was then wetted with a 25 mM solution of MeO–PEG_{50}–NH_2 and then brought into conformal contact with the wafer (Fig. 5, step 2). The stamp was then peeled off, the substrate rinsed, and then immersed in a solution of hexadecylamine to backfill the unreacted but activated regions of the substrate (Fig. 5, step 3). The C_{16}–PEG_{50} compositional pattern results in a surface energy pattern; PEG regions are hydrophilic, while hexadecylamine regions are hydrophobic. Due to the refractive index differential between the alkylated and PEGylated portions of the polymer brush, the surface pattern could be visualized under an optical microscope (Supplementary data).

As previously noted the PEG functionalized brushes have a high affinity for citrate-capped gold nanoparticles (Au NP) while alkane-functionalized brushes have a low affinity for such nanoparticles. Thus the surface energy pattern can be "developed" by immersing the substrate in an AuNP solution. Fig. 6 shows selective absorption

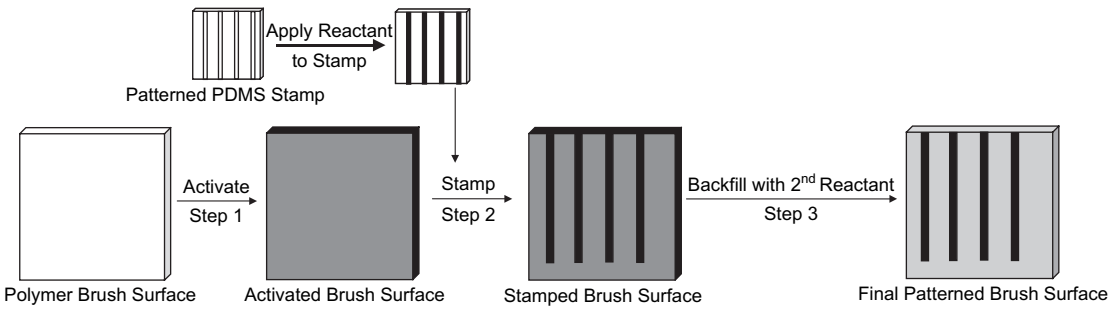

Fig. 5. Schematic of reactive microcontact printing process.

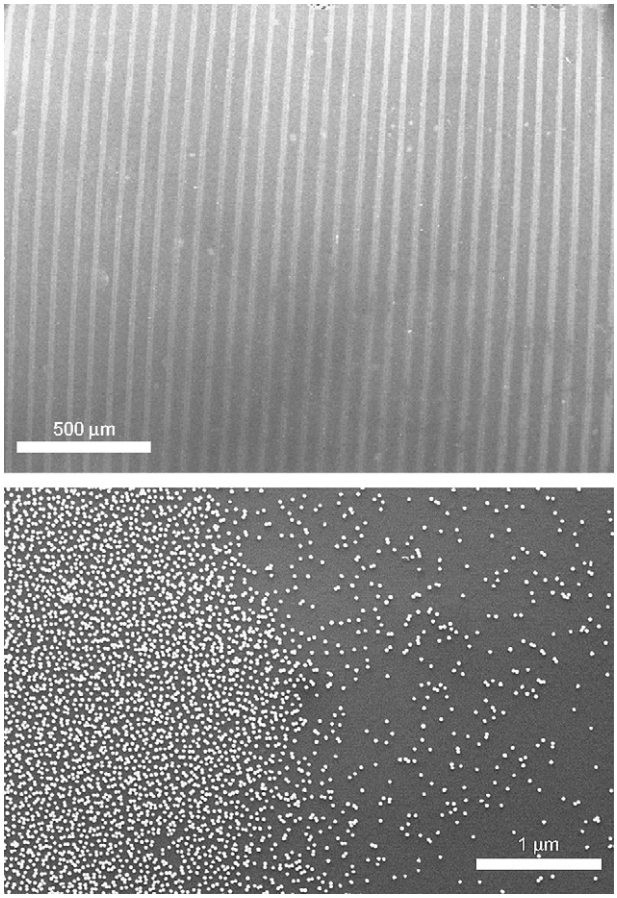

Fig. 6. Scanning electron microscopy images of reactively patterned substrate after exposure to gold nanoparticle solution. (Top) uniformity of pattern over mm^2 area. (Bottom) resolution of the edge of pattern showing abrupt transition from high areal density Au NP absorption on PHEMA-*g*-PEG_{50} to low areal density Au NP absorption on PHEMA-*g*-C_{16}.

of 30 nm citrate-capped AuNPs in the PHEMA-*g*-PEG_{50} regions after exposure for 24 h. Loosely physisorbed particles were removed by sonication for 5 min in Milli-Q water and methanol. In general the average particle density in the PHEMA-*g*-PEG_{50} regions (AuNP rich regions) was ≈160 particles/μm^2 (aerial coverage ≈ 10–15%). This is slightly higher than the 130 particles/μm^2 seen on homogeneous PHEMA-*g*-PEG_{50}. In the PHEMA-*g*-C_{16} regions (AuNP poor regions), ≈25 particles/μm^2 were observed; significantly higher than the values seen on homogeneous PHEMA-*g*-C_{16} surfaces (≈1 particle/μm^2). It is currently unclear why the R-μCP process may lead to higher nanoparticle densities than those seen on homogeneously reacted surfaces. However, there is literature precedent that reactions performed via R-μCP show enhanced yields due to the close proximity of reactants provided by the μCP geometry [14]. This could result in higher levels of coupled PEG_{50} and corresponding affinity for AuNPs. The presence of the AuNPs on the PHEMA-*g*-C_{16} regions may reflect unintentional deposition of PEG_{50} moieties prior to C_{16} grafting, such as via the recessed regions of the stamp, or more likely via transfer during the bulk rinse step intermediate between the PEG_{50} and C_{16} grafting reactions. As noted above, the coupling between α-amines and succinimide is highly efficient, occurring at very low concentrations of the α-amine reactant. Despite these unresolved issues, due to the tolerance of the post-functionalization chemistry to a wide variety of reactants, it is conceptually possible to create a large diversity of patterned surfaces. In practice, however, we find that the inking of stamps with different molecules must be individually optimized with regard to solvent and reactant concentrations in order to ensure complete and uniform coverage of the stamp.

1.3. Reactive microcapillary patterning

The activate and coupling post-functionalization approach also enables patterning via local confinement of reactants in channels. This "reactive" microcapillary patterning (R-μCaP) is conceptually similar to micromolding in capillaries (MIMIC) [19], but instead of the capillary solution cross-linking on top of the substrate, it reacts with the substrate. In our case, R-μCaP is anticipated to enable deeper penetration of reactants into the interior of the brush relative to R-μCP, due to the presence of reactants in the solvated versus dry state. That is the architecture of the post-functionalized brush will be different, brushes patterned throughout their chain length (R-μCaP) versus at the air–brush interface (R-μCP).

The R-μCaP process, schematically shown in Fig. 7, was performed as follows. The PHEMA brush was activated as previously described (Fig. 7, step 1). The channel patterned PDMS stamp was then brought into contact with the wafer, and vacuum was applied via a cavity at the end of the pattern (Fig. 7, step 2). This vacuum-

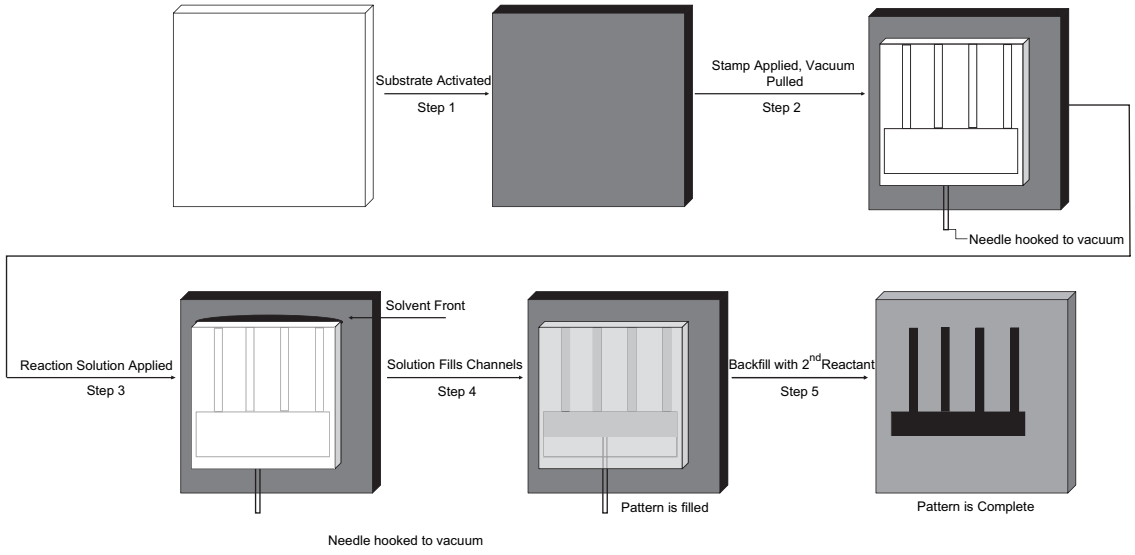

Fig. 7. Schematic of reactive microcapillary patterning process.

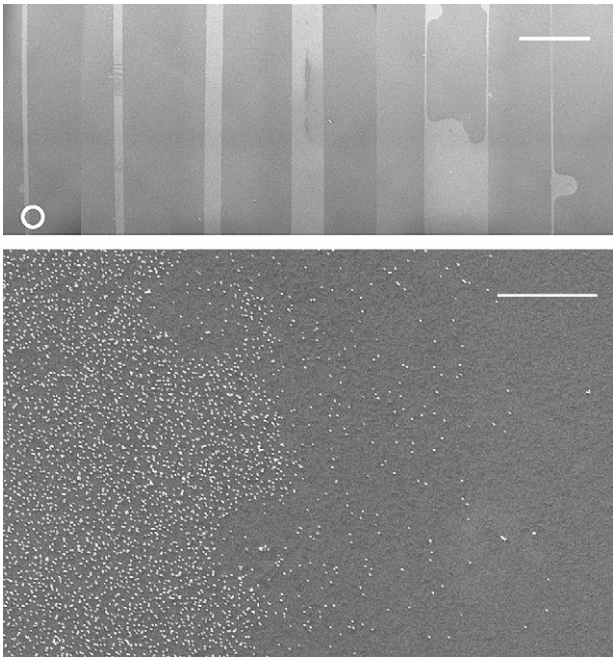

Fig. 8. Scanning electron micrographs showing areas of high and low Au NP areal densities on PHEMA-*g*-PEG_{50}–PHEMA-*g*-C_{16} surface pattern formed through reactive microcapillary patterning. (Top) fidelity of pattern across mm^2 areas, where excellent reproducibility was achieved in the smaller channels, but larger channels exhibited surfaces reflective of dewetting along the width of the channel. (Bottom) resolution of the edge of pattern (circle, top) showing abrupt transition from high areal density Au NP absorption on PHEMA-*g*-PEG_{50} to low areal density Au NP absorption on PHEMA-*g*-C_{16}. The scale bar in (Top) and (Bottom) micrograph corresponds to 500 μm and 2 μm, respectively.

assisted technique [20] avoids the complexity of a dynamically changing stamp surface that results from surface-plasma treatment of PDMS to increase hydrophilicity to enable capillary uptake of water [21]. A reservoir of an MeO–PEG_{50}–NH_2 solution in water was applied at the end of the stamp pattern (Fig. 7, step 3). After the PEG50 solution had fully percolated the channels and the solvent had evaporated (Fig. 7, step 4), the stamp was then removed from the substrate and the substrate rinsed and then immersed in a solution of hexadecylamine to backfill the unreacted but activated regions of the substrate (Fig. 7, step 5). As before the surface energy pattern was "developed" by exposure of the substrate to an Au NP solution and the substrate imaged by scanning electron microscopy (Fig. 8). Good pattern fidelity on the micron scale was achieved in the smaller channels, but larger channels exhibited surfaces reflective of dewetting along the width of the channel. The average particle density in the PHEMA-*g*-PEG_{50} regions (AuNP rich regions) was ~120 particles/μm^2, in very close agreement with the aforementioned homogeneous PHEMA-*g*-PEG_{50} surfaces (~130 particles/μm^2). The average particle density in the PHEMA-*g*-C_{16} regions (AuNP poor regions) was ~6 particles/μm^2, substantially closer to the values observed on homogeneous PHEMA-*g*-C_{16} surfaces (~1 particles/μm^2) than observed for R-μCP. Dewetting of large channels and the imprecise edge definition are due to several factors including surface energy mismatch between the stamp and the underlying brush and non-uniform swelling of the brush which can be addressed by process optimization.

2. Conclusion

A highly versatile and efficient method of polymer brush functionalization has been developed by exploiting the specificity and water tolerance of DSC-mediated coupling for side chain derivatization of PHEMA hydroxyl groups. This "activate and couple" technique has allowed us to attach a variety of synthetic molecules in order to effectively tailor the surface properties of the polymer brush. Furthermore, it has been demonstrated that this coupling reaction can be performed at short reaction times (<10 min), low solution concentrations (μM) and in various solvents, including buffer. The speed and precision of this functionalization chemistry allow the fabrication of patterned brush surfaces via "reactive" soft lithography such as R-μCaP or R-μCP. The exposure of these patterned brush surfaces to nanoparticle solutions results in replication of the surface energy pattern (based on differential binding affinity) with high fidelity at the micron scale. This represents a facile method to create hierarchically patterned hybrid polymer–nanoparticle surfaces, useful for a range of sensing applications that capitalize on the distance dependent plasmonic characteristics of gold nanoparticle arrays.

Although both pattern techniques discussed require further optimization to reach the pattern-edge fidelities seen in soft lithography on SAMs, the "activate and couple" methodology to post-functionalized polymer brushes is clearly a viable technique to create surface energy and nanoparticle density patterns on robust polymeric surfaces. Additionally, the biocompatibility of succinimide coupling enables the extension of both R-μCP and R-μCaP approaches to a wide variety of biomolecules, including peptides, proteins and enzymes. Establishing a detailed picture of correlation between reaction conditions, reactant size and the distribution of side-chain functionalities along the depth of the brush is a necessary follow-on to enable fabrication of surfaces that fully capitalize on the specificity afforded by biomacromolecules. In general, optimization of "activate and couple" methodology with reactive micro-printing processes will enable the fabrication of sophisticated multifunctional surfaces.

3. Experimental

3.1. Materials

All chemicals unless specified were analytical grade from Sigma–Aldrich and were used as-received. 2-Hydroxyethyl methacrylate (HEMA) was obtained from Acros, methanol (HLPC grade) was purchased from Fisher Scientific. CuCl and $CuCl_2$ (analytical grade) were obtained from Sigma–Aldrich and were used as-received. Citrate-capped gold nanoparticle solutions (30 nm) were used as-received from Ted Pella. MeO–PEG_{50}–NH_2 and MeO–PEG_{20}–NH_2 were used as-received from Polymer Source. 1*H*,1*H*-Perfluorooctylamine was used as-received from SynQuest Labs. *N*,*N*′-Disuccinimidyl carbonate was from Fluka (purum grade) and was used as-received.

3.2. Instrumentation

Polymer brush thicknesses were measured by ellipsometry via a Senetech SE400 variable angle ellipsometer using a wavelength of 632.8 nm and angles from 40° to 70°. Six spots per wafer were measured and the results averaged. Reported error was the spread in data from the six different measurements. Thickness was determined using the accompanying software and the measured phi and psi angles. The bulk refractive index of 1.512 for PHEMA was assumed. Note that for film thickness below 20 nm, refractive index differences in the range anticipated for the post-functionalization ($\Delta n \sim 0.1$) result in an insignificant change in the calculated thickness (±10%). Elemental compositions and coupling efficiencies were determined using ESCA 2000 software by averaging results from four spots (800 μm^2) on each wafer by X-ray photoelectron spectroscopy (XPS) performed on a Surface Instruments (SSI) M-probe instrument operated at a base pressure of 3×10^{-7} Pa using

an operating voltage of 10 kV. Contact angles were determined on an FTA200 from First Ten Angstroms at ≈22 °C. In a given experiment with a single water drop, 30 contact angle measurements were taken over 2 min and averaged. Four separate experiments were conducted per sample and these results averaged. All samples were analyzed on the same day at 15% relative humidity. Optical microscopy was performed on a Zeiss-Axio optical microscope. Gold nanoparticle patterns were imaged by an FEI XL30 scanning electron microscope at 20 kV at a working distance of 5.0 mm.

3.3. Polymer brush synthesis

Silicon wafers (Silicon Valley Microelectronics Ltd.) were cut into pieces of desired sizes and exposed to ultraviolet radiation/ozone (UVO) treatment (Jelight Inc., model 42) for 30 min. This treatment generates a large concentration of surface-bound hydroxyl groups required for the attachment of polymerization initiator. Poly(2-hydroxyethyl methacrylate) (PHEMA) brushes were prepared by "grafting from" polymerization based on atom transfer radical polymerization (ATRP) on account of its ability to form polymers with low polydispersity as described in prior publications [11a,23]. This procedure involved the deposition of the ATRP initiator (11-(2-bromo-2-methyl)propionyloxy)-undecyl trichlorosilane, (BMPUS) on the surface of silicon wafer and subsequent polymerization initiated from the surface-bound BMPUS centers. BMPUS was attached to silicon substrate by keeping UVO-treated wafer in the initiator solution (5 ml in 150 ml anhydrous toluene at −10 °C for about 12 h). Polymerization of HEMA was carried out using methanol/water ATRP using a mixture containing 37.45 g of HEMA, 25.5 g of methanol, 7 g of water, 2.33 g of bipyridine, 0.663 g of CuCl and 0.05 g of $CuCl_2$. The polymerization time (ranging between 2 and 5 h) was adjusted to achieve desired brush thickness (≈10 nm) and tethering density of ≈0.4 chains/nm^2. Note that the pristine polymer brush was characterized extensively as described in prior publications [13,23,24]. In general obtaining the grafting density of brushes on flat substrates is a challenge, since cleavage of the brushes from flat substrates liberates insufficient material for subsequent size exclusion chromatography (SEC) analysis. However, by combining ellipsometric results of dry brush thickness with SEC measurements from brushes grown on and cleaved off small particles a good estimate of the grafting density is obtained. Using this procedure a rough correlation between the brush dry thickness (h) and molecular weight (M) of the brush is established ($M = 1200h$, where h is in nanometers) [23].

3.4. Polymer brush functionalization

Note: For all reaction series, experiments were performed on a single brush wafer fractured into multiple pieces. This ensures that the measured results are not impacted by the variations of chain density or chain length on different brush wafers. Polymer brushes were immersed in a deoxygenated solution of 0.1 M *N*,*N*′-disuccinimidyl carbonate (DSC) and 4-dimethylaminopyridine (DMAP) in anhydrous dimethylformamide (DMF) for 24 h. The brushes were then rinsed thoroughly with DMF and methylene chloride and then immersed in a solution at the proper reactant concentration of the primary amine containing coupling reagent for the specified time. The brushes were then removed from the solution and sonicated for 15 min each in Milli-Q water, acetone, and methylene chloride in order to remove excess adsorbed reactants. The post-functionalized brushes were characterized by ellipsometry, water contact angle measurements, and XPS as detailed in Section 3.2. An example of the determination of elemental composition follows: for the coupling of hexadecylamine, the high resolution carbon 1s peak, oxygen 1s peak, and nitrogen 1s peak were all integrated. The ESCA 2000 software automatically determined the elemental composition by multiplying each peak area by its respective sensitivity factor and dividing it by the total for all elements present. The fitting of the carbons 1s peak was performed in an automated fashion using the peak-fitting program on the software.

3.5. Estimation of grafting efficiency

Grafting efficiencies were estimated by either carbon 1s peak fitting (in the case of PEG) or elemental composition (carbon, oxygen or fluorine), respectively, as described below. Note that due to the difficulty in integrating the relatively small nitrogen peak, nitrogen composition was not used to calculate grafting efficiency. When possible, (as in the case of hexadecylamine) estimates were performed by both carbon 1s peak fitting and elemental composition to ensure that both methods gave similar results. Assuming the post-functionalized brush is composed of unreacted (unactivated) PHEMA monomers (u) and reacted (coupled) PHEMA monomers (r), the total elemental composition, C_T, can be expressed as $C_T = C_u\chi_u + C_r\chi_r$ where C_i is the elemental content, χ_i is the fraction of reacted and unreacted monomers, and $\chi_u + \chi_r = 1$. The grafting efficiency, defined as the fraction of reacted monomers (χ_r), is then $\chi_r = (C_T - C_u)/(C_r - C_u)$. The elemental carbon composition of the pristine PHEMA brush and theoretical 100% grafted brush are summarized in Table 1. For the XPS conditions used, the escape depth of 95% of 1s electrons (defined as 3λ where λ is the inelastic mean-free path length of the surface ejected electrons) from these polymers is approximately 7.2, 6.4, and 5.7 nm for carbon, oxygen, and fluorine, respectively; this implies that the estimated efficiencies are specific for the outermost 25–33% of the brush. Finally, there was insufficient resolution to estimate the relative content of the activated PHEMA–succinimide monomer (C:O – 1.6:1) and pristine PHEMA monomer (C:O – 2:1), thus the reported estimates based on the α-amino coupled brushes reflect the efficiency of both steps and imply that DSC-activation process is of greater efficiency. This is consistent with literature reports that the amino coupling to the PHEMA–succinimide is highly efficient [8].

3.6. Reactive microcontact printing

The PDMS stamp pattern was fabricated as has been previously described [25]. Briefly, the silicon master was placed in a glass petri dish and a 10:1 (w:w) mixture of Sylgard 184 elastomer and curing agent was mixed and poured over the master. This was then degassed under vacuum to prevent air bubbles from forming in the pattern. After degassing, the stamp was then allowed to cure overnight at room temperature. After curing, the PDMS stamp was cut out by a razor blade and washed and sonicated in a mixed ethanol/water solution (30:70 v:v) prior to use and then dried in a nitrogen stream to remove unreacted monomer and contaminants. The particular PDMS pattern used for R-μCP (Supplementary data) consisted of a repetitive line pattern with raised features of 25 μm width and recessed features of 45 μm width. To activate the polymer brush, the substrate was immersed in a deoxygenated solution of 0.1 M *N*,*N*′-disuccinimidyl carbonate (DSC) and 4-dimethylaminopyridine (DMAP) in anhydrous dimethylformamide (DMF) for 24 h. The brushes were then rinsed thoroughly with DMF and methylene chloride. The PDMS stamp pattern was wetted with a 25 mM solution of $MeO–PEG_{50}–NH_2$ in acetone by application with a Q-Tip. *Note*: The PDMS stamp can also be inked via spin coating of the reactant solution or other various application methods, but it was found that the Q-tip application method yielded the best results. The PDMS stamp was then brought into conformal contact with the wafer under an applied force of 1 kg/cm^2 and was kept in contact until the interface was fully dry (≈10 min).

The stamp was then peeled off and the substrate was rinsed in acetone and methylene chloride and then immersed in a 25 mM solution of hexadecylamine in acetone in order to backfill the unreacted but activated regions of the substrate. The wafer was then sonicated thoroughly for 15 min each in Milli-Q water, acetone, and methylene chloride in order to remove excess adsorbed reactants. The wafer was then floated on a solution of citrate-capped gold nanoparticles (Ted Pella) for 24 h. The substrate was then taken out of solution and rinsed and sonicated for 5 min each in Milli-Q water and methanol to remove loosely physisorbed particles. The substrates were imaged by SEM as described in Section 3.2, and the density of AuNPs on the brush surface was quantified via image processing of the SEM images using image-J software.

3.7. Reactive microcapillary patterning

The PDMS stamp pattern was fabricated as has been previously described [22] and summarized above. The particular PDMS pattern used for R-μCaP (Supplementary data) consisted of a series of parallel channels, where each channel sequentially increased in size from the exterior (30 μm) to the center of the pattern (850 μm). Polymer brushes were activated as described above. The pristine (non-plasma treated) PDMS channel pattern was then brought into contact with the wafer. A needle connected to a vacuum line was punctured into a cavity at the end of the pattern and the vacuum was then activated, enabling conformal contact of the stamp with the substrate without applied weight. A reservoir of 100 μL of a 25 mM solution of MeO–PEG_{50}–NH_2 in water was then applied at the end of the stamp pattern (schematic shown in Fig. 7). The apparatus was left for 4 h, during which time the vacuum assisted pulling of the reaction liquid into the channels and slow evaporation of water. The stamp was then removed from the polymer brush substrate; the substrate was rinsed thoroughly with acetone and methylene chloride, and then immersed in a 25 mM solution of hexadecylamine in acetone in order to backfill the unreacted but activated regions of the substrate. The wafer was then sonicated thoroughly for 15 min each in Milli-Q water, acetone, and methylene chloride in order to remove excess adsorbed reactants. Finally, the wafer was floated on a solution of citrate-capped gold nanoparticles (Ted Pella) for 24 h. The substrate was then taken out of solution and rinsed and sonicated for 5 min each in Milli-Q water and methanol to remove loosely physisorbed particles. The substrates were imaged by SEM as described in Section 3.2, and the density of AuNPs on the brush surface was quantified via image processing of the SEM images using image-J software.

Acknowledgments

The authors would like to acknowledge the Office of Naval Research (grant# N-00014-5-01-0613) and the research group of Rajesh Naik for providing PDMS patterned stamps.

Appendix. Supplementary data

Supplementary data associated with this article can be found in the online version, at doi:10.1016/j.polymer.2008.06.020.

References

[1] Huang W, Kim JB, Bruening ML, Baker GL. Macromolecules 2002;4:1175.
[2] Senaratne W, Andruzzi L, Ober CK. Biomacromolecules 2005;23:47.
[3] (a) Ulman A. An introduction to ultrathin organic thin films: from Langmuir Blodgett to self-assembly. San Diego, CA: Academic Press; 1991;
(b) Ulman A. Chem Rev 1996;96:1533.
[4] Edmonson S, Osborne VL, Huck WTS. Chem Soc Rev 2004;33:14.
[5] Advincula RC, Brittain WJ, Caster KC, Ruhe J, editors. Polymer brushes: synthesis, characterization, applications. Germany: Wiley-VCH; 2004.
[6] (a) Lutz JF, Borner HG, Weichenhan K. Macromolecules 2002;35:1175;
(b) Xu D, Yu WH, Kang ET, Neoh KGJ. Colloid Interface Sci 2004;279:78;
(c) Harris JM, Struck EC, Case MG, Paley MS, Yalpani M, Van Alstine JM, et al. J Polym Sci Polym Chem Ed 1984;22:341;
(d) Flanagan SD, Barondes S. J Biol Chem 1975;250:1484;
(e) Harris JM. J Macromol Sci Rev Macrmol Chem Phys C 1985;25:325;
(f) Zhang MC, Kang ET, Neoh KG, Han HS, Tan KL. Polymer 1998;40:299;
(g) Tugulu S, Arnold A, Sielaff I, Johnsson K, Klok HA. Biomacromolecules 2005;6:1602;
(h) Tugulu S, Silacci P, Stergiopulos N, Klok HA. Biomaterials 2007;28:2536;
(i) Jennings GK, Brantley EL. Macromolecules 2004;37:1476;
(j) Xu FJ, Zhong SP, Yung LYL, Tong YW, Kang ET, Neoh KG. Tissue Eng 2005;11:1736;
(k) Pedone E, Li X, Koseva N, Alpar O, Brocchini S. J Mater Chem 2003;13:2825–37;
(l) Ghosh S, Basu S, Thayumanavan S. Macromolecules 2006;39:5595;
(m) Godwin A, Hartenstein M, Muller A, Brocchini S. Angew Chem Int Ed 2001;40:594.
[7] Murata H, Prucker O, Ruhe J. Macromolecules 2007;40:5497.
[8] (a) Miron T, Wilchek M. Bioconjugate Chem 1993;4:568;
(b) Ballico M, Cogoi S, Drioli S, Bonora GM. Bioconjugate Chem 2003;14:1038;
(c) Zalipsky S. Adv Drug Delivery Rev 1995;16:157;
(d) Ghosh AK, Doung TT, McKee SP, Thompson WJ. Tetrahedron Lett 1992;33:2781;
(e) Alsina J, Chiva C, Ortiz M, Rabanal F, Giralt E, Albericio F. Tetrahedron Lett 1997;38:883;
(f) Christian NA, Milone MC, Ranka SS, Li G, Frail PR, Davis KP, et al. Bioconjugate Chem 2007;18:31;
(g) Hermanson GT. Bioconjugate techniques. San Diego: Academic Press; 1996 [chapter 15];
(h) Hofstetter O, Lindstrom H, Hofstetter H. Anal Chem 2002;74:2119;
(i) Wilchek M, Miron T. Appl Biochem Biotechnol 1985;11:191;
(j) Guillier F, Orain D, Bradley M. Chem Rev 2000;100:2091;
(k) Haginaka J, Seyama C, Kanasugi N. Anal Chem 1995;67:2539;
(l) Lee S, Greenwald RB, McGuire J, Yang K, Shi C. Bioconjugate Chem 2001;12:163;
(m) Vrudhula VM, Senter PD, Fischer KJ, Wallace PM. J Med Chem 1993;36:919;
(n) Greenwald RB, Zhao H, Xia J, Martinez A. J Med Chem 2003;46:5021;
(o) Rawale S, Hrihorczuk LM, Wei WZ, Zemlicka J. J Med Chem 2002;45:937;
(p) Greenwald RB, Choe YH, Conover CD, Shum K, Wu D, Royzen M. J Med Chem 2000;43:475;
(q) Andresen TL, Davidsen J, Begtrup M, Mouritsen OG, Jorgensen K. J Med Chem 2004;47:1694;
(r) Florent JC, Dong X, Gaudel G, Mitaku S, Monneret C, Gesson JP, et al. J Med Chem 1998;41:3572.
[9] (a) Alsina J, Rabanal F, Chiva C, Giralt E, Albericio F. Tetrahedron 1998;54:10125;
(b) Bocking T, Kilian KA, Hanley T, Ilyas S, Gaus K, Gal M, et al. Langmuir 2005;21:10522;
(c) Huang K, Lee BP, Ingram DR, Messersmith PB. Biomacromolecules 2002;3:397;
(d) Zalipsky S. Bioconjugate Chem 1995;6:150.
[10] (a) Cho CY, Moran EJ, Cherry SR, Stephans JC, Fodor SPA, Adams CL, et al. Science 1993;261:1303;
(b) Moran EJ, Wilson TE, Cho CY, Schultz PG. Biopolymers (Peptide Science) 1995;37:213;
(c) Paikoff SJ, Wilson TE, Cho CY, Schultz PG. Tetrahedron Lett 1996;37:5653.
[11] (a) Bhat RR, Chaney BN, Rowley J, Liebmann-Vinson A, Genzer J. Adv Mater 2005;17:2802;
(b) Mei Y, Wu T, Xu C, Langenbach KJ, Elliott JT, Vogt BD, et al. Langmuir 2005;21:12309;
(c) Yoshikawa C, Goto A, Tsujii Y, Fukuda T, Kimura T, Yamamoto K, et al. Macromolecules 2006;39:2284.
[12] Robinson KL, Khan MA, de Paz Báñez MV, Wang XS, Armes SP. Macromolecules 2001;34:3155.
[13] Wu T, Efimenko K, Vlček Petr, Šubr Vladimír, Genzer J. Macromolecules 2003;36:2448.
[14] Bhat RR, Genzer J, Chaney BN, Sugg HW, Liebmann-Vinson A. Nanotechnology 2003;14:1145.
[15] (a) Xia Y, Whitesides GM. Angew Chem Int Ed 1998;37:551;
(b) Xia Y, Rogers JA, Paul KE, Whitesides GE. Chem Rev 1999;99:1823.
[16] (a) Yan L, Huck WTS, Zhao XM, Whitesides GM. Langmuir 1999;15:1208;
(b) Sullivan TP, Maaike LP, Dankers PYW, Huck WTS. Angew Chem Int Ed 2004;43:4190;
(c) Rozkiewicz DI, Janczewski D, Verboom W, Ravoo BJ, Reinhoudt DN. Angew Chem Int Ed 2006;45:5292;
(d) Rozkiewicz DI, Kraan Y, Werten MWT, deWolf FA, Subramaniam V, Ravoo BJ, et al. Chem Eur J 2006;12:6290;
(e) Rozkiewicz DI, Ravoo BJ, Reinhoudt DN. Langmuir 2005;21:6337;
(f) Xiao PF, He NY, Liu ZC, He QG, Sun X, Lu ZH. Nanotechnology 2002;13:756.
[17] Sullivan TP, Huck WTS. Eur J Org Chem 2003;17 and references therein.
[18] (a) Hyun J, Zhu Y, Liebmann-Vinson A, Beebe Jr TP, Chikoti A. Langmuir 2001;17:6358;
(b) Lahann J, Balcells M, Rodon T, Lee J, Choi IS, Jensen KF, et al. Langmuir 2002;18:3632;

(c) Feng CL, Vansco GJ, Schonherr H. Adv Funct Mater 2006;16:1306;
(d) Feng CL, Vansco GJ, Schonherr H. Langmuir 2007;23:1131;
(e) Feng CL, Embrechts A, Bredebusch I, Schnekenburger J, Domschke W, Vansco GJ, et al. Adv Mater 2007;19:286;
(f) Burnham MR, Turner JN, Szarowski D, Martin DL. Biomaterials 2006;27:5883;
(g) Lee KB, Kim DJ, Lee ZW, Woo SI, Choi IS. Langmuir 2004;20:2531.
[19] (a) Kim E, Xia Y, Whitesides GM. J Am Chem Soc 1996;118:5722;
(b) Xia Y, Kim E, Whitesides GM. Chem Mater 1996;8:1558;
(c) Huang W, Li J, Xue L, Xing R, Luan S, Luo C, et al. Colloids Surf A Physicochem Eng Aspects 2006;278:144.
[20] Jeon NL, Choi IS, Xu B, Whitesides GM. Adv Mater 1999;11:946.
[21] Bodas D, Khan-Malek C. Sens Actuators B 2007;123:368.
[22] (a) Bhat RR, Tomlinson MR, Wu T, Genzer J. Adv Polym Sci 2006;198:51;
(b) Patten TE, Matyjaszewski K. Adv Mater 1998;10:901.
[23] Tomlinson MR, Genzer J. Langmuir 2005;21:11552.
[24] Wu T, Efimenko K, Genzer J. J Am Chem Soc 2002;124:9394.
[25] Kumar A, Biebuyck HA, Whitesides GM. Langmuir 1994;10:1498.